ChemPhotoChem

Research Article
doi.org/10.1002/cptc.202300329

Chemistry Europe
European Chemical Societies Publishing

www.chemphotochem.org

The impact of Activation on the Performance of Optical Oxygen Sensing with the Luminescent Metal–Organic Framework MOF-76(Eu)

Thomas Kasper,[a] Julian Burkhart,[a] and Klaus Müller-Buschbaum*[a, b]

The influence of activation as key parameter for oxygen sensing by luminescent metal–organic frameworks has been investigated and quantified for the archetype MOF-76(Eu). Activation at different conditions (regarding temperature and solvent-exchange for distinct vacuum pressure and heating time), shows an influence on the overall quenching, response time and cyclability due to different pore accessibility and surface area and therefore on the overall performance of the sensor. The optical sensing process is based on luminescence quenching, analyzed from high vacuum (10^{-7} bar) to ambient pressure by dosing oxygen from 0.01 bar to 1 bar. Strong influence of the different activation parameters is observed, as MOF-76(Eu) activated at 50 °C shows limited quenching of the luminescence intensity within 30 min, while methanol-exchange and subsequent activation at 250 °C leads to a quenching rate of 98.6 %. In addition, the sensor response occurs more than 1000 times faster within 0.2 s. These results correlate well with physisorption data, which reveal a significant change in porosity and surface area according to the degree of activation. For a better understanding of the involved processes, adsorption isotherms were recorded, surface areas determined and correlated to the photophysical parameters, including Stern-Volmer kinetics and cycling experiments for the differently activated MOF sensors.

Introduction

Optical sensors have developed into a widely investigated topic within the field of gas sensing.[1–3] They allow to detect various gases, e.g. oxygen,[4–6] carbon dioxide[7–9] or hydrogen sulfide,[10,11] just by the bare eye without the need for a detector. In case a separate detector is needed, they possess a high sensibility ranging down to ppb range[12,13] being competitive to other types of sensors. Furthermore, the detector can be placed outside of the measured atmosphere allowing measurements in a closed vessel through a window.[14] The detection mechanism of optical sensors bases on many different principles fitting to the corresponding analytes, e.g. luminescence quenching,[15,16] UV-vis absorption,[17] Raman scattering[18] or plasmon resonance,[12] which enables a high selectivity. In contrast, resistive semiconducting sensors always suffer from a cross sensitivity to other gases, because their working principle bases on a changed oxygen concentration adsorbed on the surface due to reduction or oxidation.[19] Because of its oxidative nature and presence in the atmosphere, sensing oxygen is of great interest and optical sensing provides a method to see its presence with the bare eye. For daily use, embedding these sensors in packaging materials of oxygen sensitive compounds could be an interesting example for application.

Different materials were investigated for optical oxygen sensing, e.g. complexes[20] or metal–organic frameworks,[21,22] but there are also examples of inorganic materials showing optical response to oxygen.[5,23–25] A large part of the sensors using luminescence as observable consist of organic molecules,[5,6,20,21,26–33] which play a significant role in the oxygen sensing mechanism: excitation with UV radiation leads to a transfer of the molecule from its singlet ground state to the excited triplet state. In absence of oxygen this is followed by other energy transfer processes, which end in emission of visible light, e.g. after energy transfer to a luminophore. If oxygen is present, the organic molecule in its excited triplet state transfers its energy to oxygen, which is converting from triplet to singlet state.[34] Since this mechanism is very specific and requires compatible energy levels, the selectivity of these sensors is high. Metal–organic frameworks are a class of materials using this kind of mechanism, too, and due to their porous structure, bring some advantages. The high porosity is accompanied by a large surface area, which at the same time is the interface for interactions with other species. Furthermore, it is possible to tune the properties of the pores, e.g. size and hydrophobicity, to adapt them to the desired analyte.[35,36]

MOFs very often only possess intrinsic luminescence due to the fluorescence of their ligands, which can be poorly visible. Therefore, many reports use post-synthetic modification with

[a] T. Kasper, J. Burkhart, Prof. Dr. K. Müller-Buschbaum
Institute of Inorganic and Analytical Chemistry
Justus Liebig University
Heinrich-Buff-Ring 17, 35392 Giessen
E-mail: kmbac@uni-giessen.de

[b] Prof. Dr. K. Müller-Buschbaum
Center for Materials Research (LAMA)
Justus Liebig University
Heinrich-Buff-Ring 16, 35392 Giessen

Supporting information for this article is available on the WWW under https://doi.org/10.1002/cptc.202300329

luminophores to obtain strongly luminescent compounds for use as sensors. In some of the earlier reports, Ir-, Ru- and Pt-complexes were used as luminophore and also act as interaction site towards oxygen.[37–42] Also, Eu-complexes were embedded into MOFs and took advantage of the characteristic, red luminescence auf trivalent europium.[43] Lanthanide-based luminescence by post-synthetic impregnation with their salts, e.g. nitrates, was also achieved.[34,44,45] There are also examples of luminescent oxygen sensing that do not rely on post-synthetic modification using MOFs based on a silver cluster,[6] lanthanides[27,28,46] or other metal centers.[21,29,31–33] All this work showed the potential of optical oxygen sensing with luminescent MOFs, e.g. through quenching rates of 96.5 %,[21] cycling for ten cycles and more,[6,37,39] or cross sensitivity.[21,30,39] A response time of several seconds was observed in some cases[31,34] with the fastest being 0.3 s.[6] In contrast, also much slower response times were reported, e.g. 53 s.[34] A fast response time is crucial for the sensor to be used without a detector since fast changes are easier recognizable by the eye. Consequently, a more detailed investigation on the parameters influencing response time and quenching is necessary to better understand the influence of the fundamental parameters involved. In a study on resistive hydrogen gas sensing with MOF-74(Co), a higher surface area was identified to have an influence on the performance of MOF-74(Co) variants[47] with the sensitivity towards hydrogen being much lower without activation of the MOF. Consequently, this work focuses on a parameter crucial for the accessibility of the interaction sites: activation of the MOF.

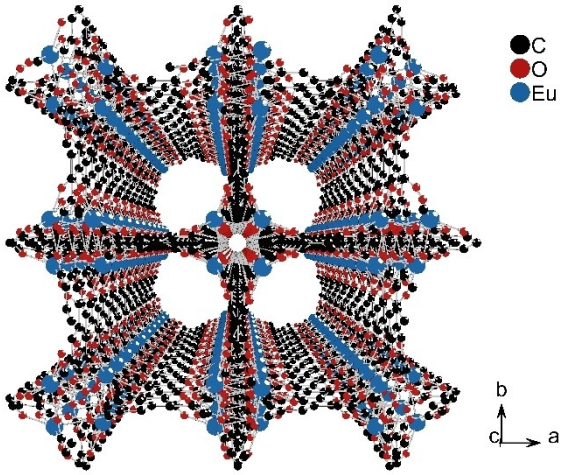

Scheme 1. Crystal structure of MOF-76(Eu), fully activated with accessible pore system. Hydrogen omitted for clarity. Depiction based on the structure reported in ref. [49].

Results and Discussion

In a previous study on luminescent oxygen sensing with MOFs,[4] we observed a weak quenching of the photoluminescence emission of MOF-76(Eu) and thereby a weaker sensitivity compared to other investigated MOFs. Therefore, we selected MOF-76(Eu) for this study, in which we identified and describe the reasons for this observation by deliberate investigation on the influence of the activation parameters and pore loading on the sensing of oxygen gas with this archetype metal–organic framework. Hence, MOF-76(Eu) was synthesized according to a modified procedure from literature[48] and activated by heating in vacuum at different temperatures to achieve different surface areas and pore accessibilities. Another procedure included a solvent exchange with methanol to remove all residues of dimethylformamide (DMF) from the pores. Other parameters (dynamic vacuum with a pressure of 10^{-6} bar and heating time of 15 h) were kept constant. MOF-76(Eu) is build up by trivalent europium ions, which are connected by 1,3,5-benzenetricarboxylic acid to form the three-dimensional, microporous structure (Scheme 1). This porosity results in a large interface for interaction with other molecules, e.g. gases, but access to this surface can also be blocked by solvent molecules inside the pores as well as surface covering molecules and solids. Although there are a significant number of publications on luminescent oxygen sensing with MOFs,[27,28,32,34,42,44] none of them focuses on the influence of pore accessibility on the overall luminescence intensity quenching and the response time of the sensor. Thus, oxygen sensing measurements were carried out by dosing oxygen to the MOF starting with high vacuum (10^{-7} bar) and measuring the change of emission intensity over time for six different oxygen pressures from 0.01 bar to 1 bar. For a better understanding of the involved processes, adsorption isotherms were recorded and surface areas determined to be correlated to the results of photoluminescence (PL) spectroscopy.

Properties of Synthesized MOF-76(Eu)

For creation of samples with different surface area and pore accessibility, MOF-76(Eu) was synthesized and then activated in dynamic vacuum (10^{-6} bar) at different temperatures (50 °C, 100 °C, 150 °C and 250 °C). Additionally, another sample was prepared by methanol-exchange and subsequent heating in dynamic vacuum (10^{-6} bar) at 250 °C. After this procedure, the samples were transferred into an argon glovebox to protect them from ambient atmosphere.

MOF-76(Eu) was successfully synthesized according to a procedure from literature,[48] which was modified by addition of hydrochloric acid for better crystallinity, as can be seen in the powder diffractograms depicted in Figure 1. No foreign reflections are observed or can be assigned to the reactants and the positions of the reflections fit to the simulated pattern of MOF-76(Eu). However, the intensity ratios of the reflections are different, which may be explained by residual solvent in the pores of the synthesized MOF-76(Eu) compared to the simulated structure, which does not contain solvent in its pores.[50,51]

Under a UV lamp, MOF-76(Eu) shows strong, red luminescence, which is characteristic for trivalent europium and caused by its parity forbidden 4f–4f transitions. The photoluminescence

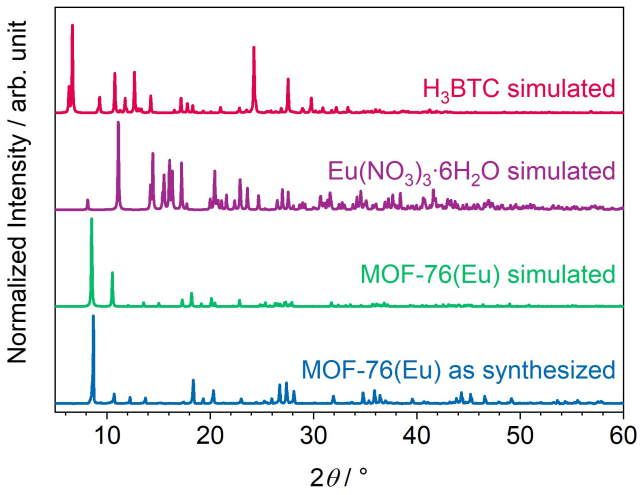

Figure 1. Powder x-ray diffractogram of synthesized MOF-76(Eu) compared to simulated diffractograms of MOF-76(Eu)[49] and reactants.[52,53]

spectra in Figure 2 were measured to confirm this observation. Since the 4f–4f transitions are parity forbidden, it is hardly possible to directly excite trivalent europium, because the light uptake is weak. Therefore, excitation mostly occurs via excitation of the ligand, followed by intersystem crossing and energy transfer from triplet states of the ligand (so called antenna effect) to excited states of Eu^{3+}, from which emission occurs. This is observed as a broad band in the excitation spectra. But the forbiddance of direct excitation is not strict and thus sharp lines corresponding to this can be seen. The emission spectra of MOF-76(Eu) also show sharp lines caused by the already mentioned narrow-banded 4f–4f transitions. The 4f orbitals of the lanthanides are shielded very well by the outer 5d orbitals and therefore they are not influenced by chemical surroundings leading to these transitions to be found at the same energy. The strongest signal corresponds to the transition

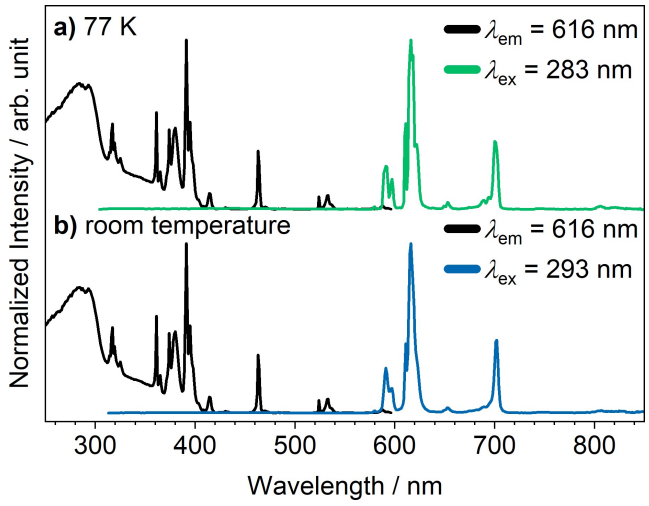

Figure 2. Photoluminescence excitation (black) and emission (colored) spectra of as synthesized MOF-76(Eu) at a) 77 K (green) and b) room temperature (blue).

$^5D_0 \rightarrow {}^7F_2$ at 616 nm and is also the main reason for the red color of the emission. Trivalent europium possesses some unique luminescence characteristics separating it from the other lanthanides, e.g. hypersensitive transitions. Although the 4f orbitals are shielded very well, some of them do possess a sensitivity to the chemical surrounding. In case of the aforementioned transition $^5D_0 \rightarrow {}^7F_2$, this results in a splitting of the transition bands due to the different coordination spheres of Eu^{3+} in the structure of MOF-76(Eu).

To complete the determination of the photoluminescence properties of MOF-76(Eu), emission lifetime and quantum yield were determined (Table 1). The overall process decay time (lifetime) for the Eu^{3+} emission maximum at room temperature is 0.717(5) ms and slightly prolonged to 0.769(6) ms at 77 K due to decreased thermal quenching. These lifetime values, as well as the quantum yield of 14(3)% are in the same range as reported in the literature.[49,54,55]

Effects of Activation on MOF-76(Eu)

After activation, another powder diffractogram of the MOF was recorded to monitor possible changes introduced by the activation procedure (Figure 3). Since MOFs are known for changing the intensity ratios of the reflections with different pore fillings, this also provides first information about the degree of activation upon heating at different temperatures. While for as-synthesized MOF-76(Eu), the reflections at higher 2θ have distinct well observable intensity, they are reduced in intensity relative to the main reflection (100) at 2θ of 8.7° after activation, e.g. for methanol-exchanged MOF-76(Eu), with all reflections but the main reflection requiring an enlarged scaling to be clearly identified. The intensity distribution for the main Miller indexes is summed up regarding reflections identifying the direction of the *a*-axis [100]. As a result, the relative intensity of reflections at higher 2θ is decreasing with an increased activation temperature and the lowest intensity is obtained for the methanol exchanged MOF-76(Eu) (Figure 3b). Furthermore, the main reflection is shifted to higher 2θ at increased temperatures (e.g. 8.9° after activation at 50 °C) indicating a contraction of the whole structure due to removal of the solvent, but shifting back to lower 2θ with further increased activation temperature. The higher temperature and especially the solvent-exchange with low-boiling methanol results in a removal of most of the solvent in the pores. The initially observed contraction could be due to interactions of the framework with the reduced amount of solvent within the

Table 1. Photoluminescence emission lifetimes at room temperature and 77 K, and quantum yield of as synthesized MOF-76(Eu).

Temperature	τ / ms	Φ / %
Room temperature	0.717(5)[a]	14(3)[c]
77 K	0.769(6)[b]	–

[a] λ_{ex} = 293 nm, λ_{em} = 616 nm. [b] λ_{ex} = 283 nm, λ_{em} = 616 nm. [c] λ_{ex} = 310 nm, λ_{em} = 500 nm–725 nm.

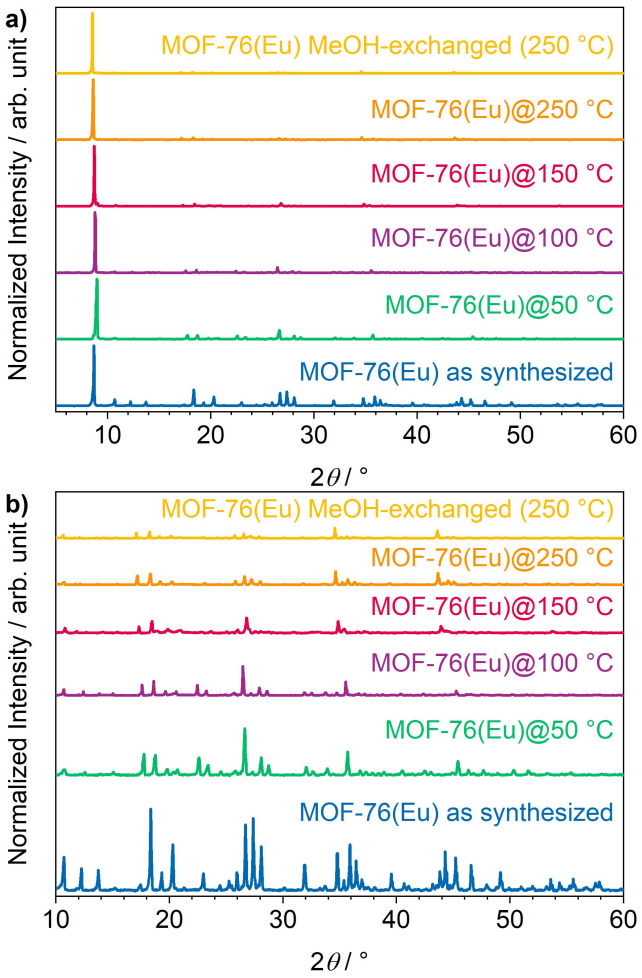

Figure 3. a) Powder x-ray diffractograms of as-synthesized MOF-76(Eu) compared to MOF-76(Eu) activated at different conditions; b) respective diffractograms with a selected range in 2θ view for a better representation of low reflection intensities.

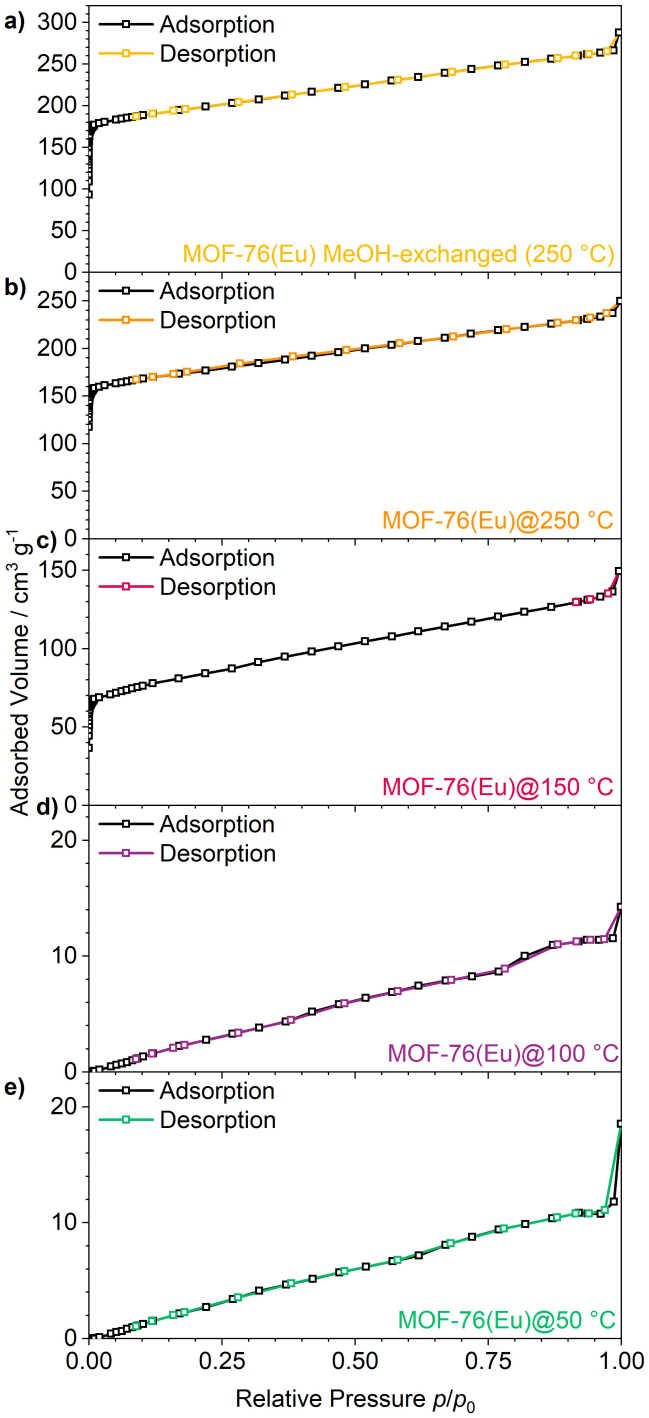

Figure 4. Nitrogen adsorption and desorption isotherms of MOF-76(Eu) activated under different conditions. Desorption isotherm of MOF-76(Eu)-@150 °C could not be fully measured because of experimental limitations due to long equilibration times.

pores, whereas for nearly full removal, these interactions disappear and lead to a re-expansion of the framework. For methanol exchanged MOF-76(Eu), a reflection at 2θ of 8.5° was observed after activation at 250 °C.

For evaluation of the activation, physisorption measurements were carried out, which can give information about the surface area and pore size. As synthesized MOFs contain residues of solvent within their pores. The latter can therefore be blocked and should not be available during physisorption. After activation, the pores are accessible and contribute to a higher surface area. The adsorption and desorption isotherms for MOF-76(Eu) activated at different temperatures (while keeping all other activation conditions constant to a vacuum of 10^{-6} bar and a heating time of 15 h) are depicted in Figure 4. After activation at 50 °C and 100 °C, type II isotherms were observed, but with overlap between mono- and multilayer adsorption due to low interaction between adsorbate and adsorbent (see also supporting information for more details on physisorption data and BET fits). Estimation of the surface area via the BET method gives values of 16 $m^2 \cdot g^{-1}$ and 17 $m^2 \cdot g^{-1}$ for activation at 50 °C and 100 °C, respectively, indicating that the pore system is not to hardly available. At 150 °C and above this changes drastically, the adsorption isotherm shows a high uptake of nitrogen at low p/p_0 indicating microporosity. A BET surface area of 256 $m^2 \cdot g^{-1}$ further confirms this result. Residual solvent molecules start to evaporate from the pores at temperatures of 150 °C and above in vacuum and lead to accessibility

of the pores. After activation at 250 °C, MOF-76(Eu) takes up even more nitrogen exhibiting a surface area of 686 $m^2 \cdot g^{-1}$. This is comparable to results observed in the literature[56,57] and indicates that most residual DMF molecules have been removed. However, methanol-exchange of MOF-76(Eu) for three days before activating it by heating in vacuum leads to an even higher surface area of 768 $m^2 \cdot g^{-1}$ due to the lower boiling point of methanol in comparison to DMF.

The results of elemental analysis (Table 2) confirm the results of the physisorption showing an increasing agreement with the calculated values for proceeding activation up to the fully methanol-activated MOF-76(Eu). A lack of activation as well as incomplete activation can also be seen by the presence of nitrogen and additional carbon and hydrogen content due to DMF inside the pores of MOF-76(Eu). The similar DMF content in MOF-76(Eu)@50 °C and MOF-76(Eu)@100 °C displays that no reasonable activation can be achieved up to 100 °C, which is also in agreement with the physisorption results, as well as starting activation and lower DMF content for MOF-76(Eu)-@150 °C resulting in a certain accessibility of micropores during the respective physisorption measurements. Results of elemental analysis are further confirmed by DTA/TG-MS (see supporting information), in which DMF was detected for MOF-76(Eu) activated below 150 °C, but not for activation conditions at 250 °C.

Effects of Activation on MOF-76(Eu) as O_2 Sensor

Oxygen pressure dependent photoluminescence spectra were recorded to investigate, if the overall luminescence emission quenching correlates with the activation temperature. The photoluminescence emission spectra shown in Figure 5 were recorded 90 min after dosing oxygen to ensure equilibration of the diffusion processes and completion of the quenching process. Furthermore, they show that the presence of oxygen leads to some quenching regardless of the activation temperature. This indicates that all forms of the MOF, no matter if activated or not, in principle, are oxygen sensors. However, the degree of PL intensity quenching is very different and dependent on the degree of activation, e.g. for samples activated at 150 °C and above. Quantitatively, insufficient activation of MOF-76(Eu) at 50 °C leads to a luminescence emission quenching of

Table 2. Elemental composition (CHN) of MOF-76(Eu) activated at different temperatures. The degree of activation is depicted by the match (top) as well as mismatch (bottom) with the calculated values.

Sample	C/%	H/%	N/%
MOF-76(Eu) calculated[a]	28.7	1.3	–
MOF-76(Eu) MeOH-exchanged (250 °C)	29.8	1.5	–
MOF-76(Eu)@250 °C	30.2	1.1	–
MOF-76(Eu)@150 °C	30.8	1.5	0.7
MOF-76(Eu)@100 °C	33.4	2.6	3.3
MOF-76(Eu)@50 °C	33.4	2.5	3.2

[a] Calculated for composition [Eu(BTC)(H_2O)] ($EuC_9H_5O_7$).

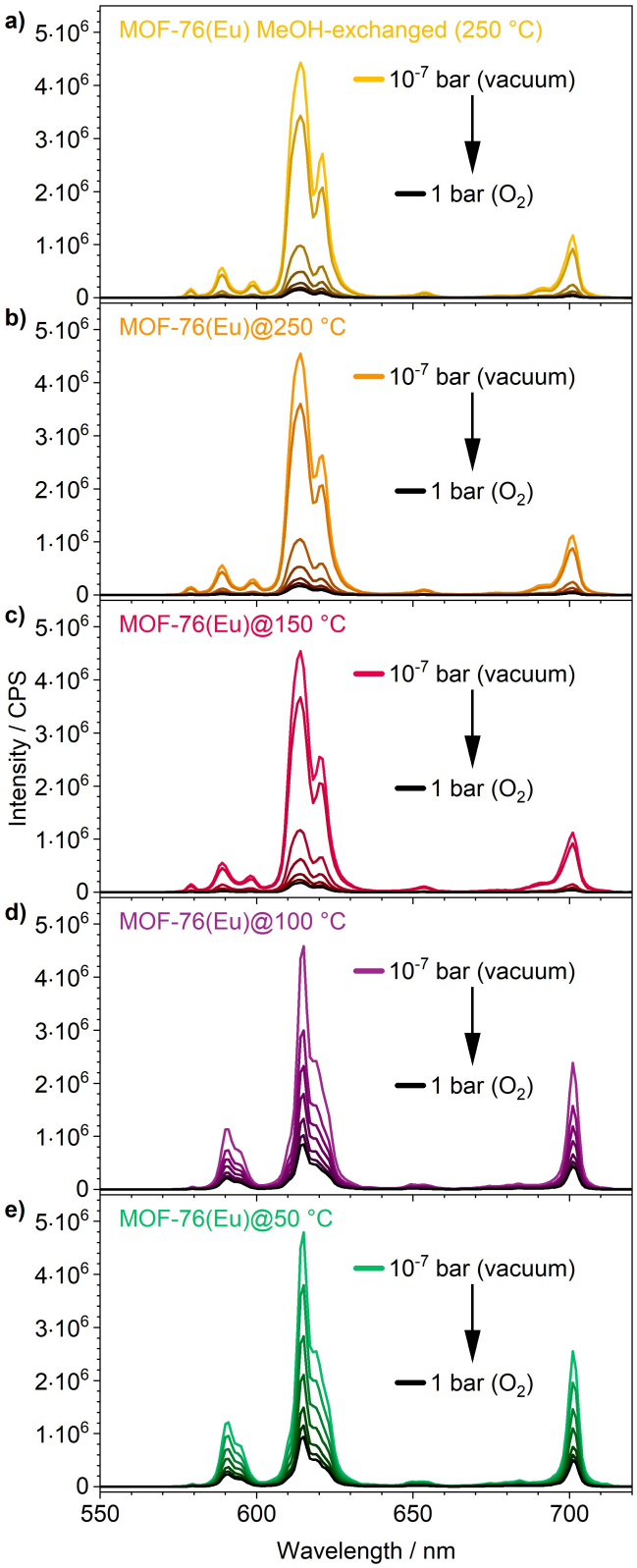

Figure 5. Oxygen pressure dependent quenching of photoluminescence emission intensity for MOF-76(Eu) activated at different temperatures. Spectra measured 90 min after dosing oxygen to sample. Oxygen pressures: 0.01 bar, 0.1 bar, 0.25 bar, 0.5 bar, 0.75 bar and 1 bar.

80.3% (Figure 6). Interestingly, after treatment at 100 °C, the quenching rate is almost similar with 80.7%. A larger change is observed after activation at 150 °C, which is enough to increase the quenching to 96.2%. When going to a further increased activation temperature of 250 °C, quenching reaches 96.8% of the emission intensity. Non-accessibility of the pores being partly blocked by residual DMF from the synthesis explains the lower quenching rate – however, oxygen can still interact with the MOF luminophores and quench the emission to a certain extent. Although MOF-76(Eu) was heated in vacuum and therefore the boiling point was lowered from 153 °C at ambient atmosphere, the conditions were not sufficient for completely removing DMF from the pores. This already shines light on a crucial point of oxygen sensing with metal–organic frameworks, which is not discussed in the literature yet: varying sensing results due to differing activation parameters. When a methanol-exchange of the solvent was carried out before activation at 250 °C, a further increase of the quenching rate is observed with 98.6%, being already close to almost no emission at all. This observation fully agrees with the physisorption results since blocked pores at lower activation temperatures (50 °C, 100 °C) lead to a lower accessible surface area and therefore lower photoluminescence emission quenching. The accessibility of the micropores after activation at higher temperatures (150 °C, 250 °C) and methanol-exchange (250 °C) results in a stronger quenching, but the quenching is not fully scaling with the increase in the BET surface area, which shows a major increase from an activation temperature of 150 °C to 250 °C compared to activation at 250 °C to methanol-exchanged MOF-76(Eu). These observations imply that oxygen is able to interact with the inner surface of the MOF even after insufficient activation below 150 °C. However, since oxygen needs to diffuse through the residual DMF in the pores, which is also occupying some of the pore space (leaving less for oxygen and its interaction with the MOF), it is not possible to reach full quenching without accessibility to the pores by removal of the solvent. At a certain degree of activation, enough solvent is removed to open most of the pores. Removal of the last residuals of solvent results in an optimization of the quenching by giving access to the last unblocked quenching sites. Therefore, it can be assumed that accessing the inner surface is more important for a complete quenching than full removal of the solvent.

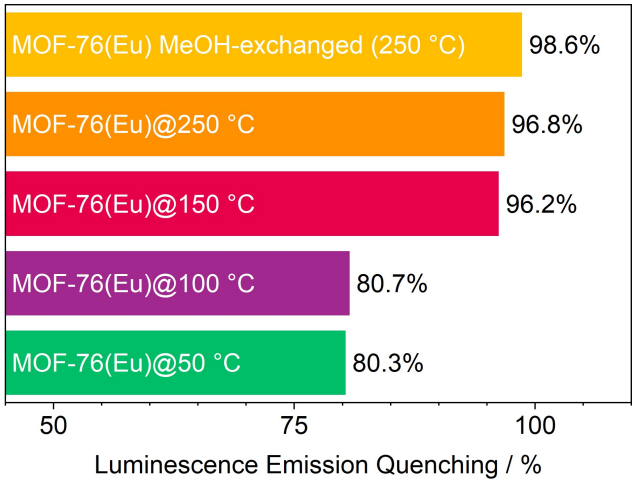

Figure 6. Comparison of emission intensity quenching for MOF-76(Eu) activated at different temperatures.

For a better understanding of the observations above, also time-resolved photoluminescence emission spectra were recorded (Figure 7). These measurements were conducted on two different time scales: recording of full spectra every 3 min (for 90 min) and monitoring the emission maximum of Eu^{3+} ($\lambda_{max} = 614$ nm) with an integration time of 0.1 s. The full spectra were integrated to consider the whole emission intensity and are depicted as single points. To ensure that no shift of the emission line maxima influences the investigations, the wavelength position of the transition maxima was monitored with full spectral analysis. For MOF-76(Eu) samples treated at 50 °C and 100 °C, full spectra were recorded every 3 min after each oxygen dosing (Figure 7a–b). In both cases, the intensity decreases within 30 min and then stays at a certain value. In opposite, the time-resolved emission spectra of MOF-76(Eu) outgassed at 150 °C and above (incl. methanol-exchanged sample) do not show such a decrease at this timescale, but on a shorter timescale within 5 s. The emission quenching process is so fast that it occurs instantly. The corresponding results are depicted in Figure 7c–e and show intensity decreases occurring within seconds, e.g. 2.9 s for dosing 0.01 bar oxygen into a vacuum of 10^{-7} bar or only 0.2 s for going from 0.75 bar to 1 bar (MOF-76(Eu) activated at 250 °C), and therefore responding faster than MOF-76(Eu) activated below 150 °C by a factor more than 1000. Furthermore, it shows that the process is on the same timescale for all three samples activated at 150 °C and above (incl. methanol exchanged), further confirming that pore accessibility is playing a larger role compared to total surface area. The observations above correlate with the observations in the physisorption measurements, which showed no porosity for the samples activated at 50 °C and 100 °C, while at 150 °C and above the micropores were observed to be accessible. In the latter case, no or less solvent is present inside the pores resulting in the easiest accessibility due to a high surface area for oxygen to interact with. In case of the samples activated at 50 °C and 100 °C, the pores are blocked by solvent molecules and therefore the interaction site is way lower. One assumption can be that luminescence emission quenching in these two samples only occurs at the outer surface area, but its accessibility in general is good, but does not explain the slow response time to oxygen in comparison to well-activated samples. Another assumption is that the inner surface area of the two samples activated at 50 °C and 100 °C is hardly, but still accessible, because diffusion through residual solvent is possible. Since diffusion in liquids is slower in comparison to the gas phase this would explain the slow response time. Since the physisorption analysis was carried out at 77 K, there is not enough energy for diffusion processes through liquids and the micropores of MOF-76(Eu) cannot be accessed and therefore were not observed. Moreover, the temperature is far below the melting point of DMF,

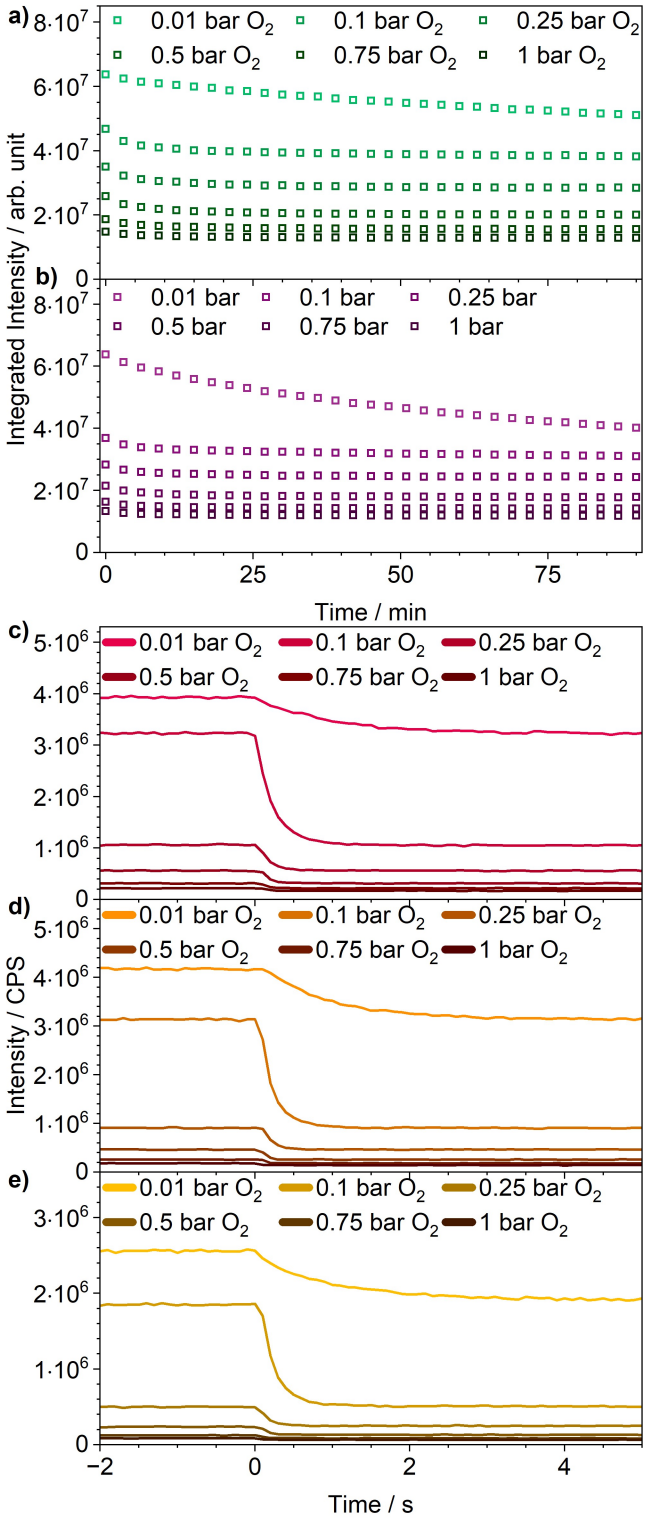

Figure 7. Quenching of photoluminescence emission at different oxygen pressures over time for MOF-76(Eu) activated at a) 50 °C, b) 100 °C, c) 150 °C, d) 250 °C and e) methanol-exchanged at 250 °C.

which will act as an even larger diffusion barrier due to this fact. Another observation of the time-resolved measurements is that the response time at low pressures is longer than at higher pressures, which can be seen very well for the measurements carried out at an oxygen pressure of 0.01 bar. There are several factors that add to this observation: firstly, at higher pressures the driving force to enter the pores increases due to the larger pressure difference and therefore the intensity change, e.g., from 0.75 bar to 1 bar occurs faster than from 10^{-7} bar to 0.01 bar. Furthermore, an increasing oxygen pressure is accompanied by a higher oxygen concentration also contributing to the faster quenching.

The process behind optical oxygen sensing in metal–organic frameworks is usually described according to Stern-Volmer kinetics, which was selected accordingly. It expresses the correlation between the presence of a foreign gas and the luminescence emission intensity based on molecule collision:[58]

$$\frac{I_0}{I} - 1 = k_q \tau_0 \cdot [Q] = K_{SV} \cdot [Q] = K_{SV} \cdot p(Q) \quad (1)$$

In equation (1), I_0 corresponds to the intensity in absence of the quencher Q, I is the emission intensity at a given quencher concentration [Q] (or partial pressure p(Q)) and K_{SV} is the Stern-Volmer constant. K_{SV} gives a value for the strength of quenching since it is the product of quenching constant k_q and the emission lifetime in absence of the quencher τ_0. Stern-Volmer plots are calculated from the quenching data and thus also influenced by changes in quenching intensity occurring with ongoing time. This can be seen in Figure 8d–e, in which the slope of the linear fits 3 min after dosing oxygen is lower than after 45 min or 90 min (compare also Table 3). Since the slope of the fits correspond to K_{SV}, its value increases with ongoing time, e.g. for MOF-76(Eu) activated at 50 °C a value of 3.47 bar^{-1} was obtained after 3 min, which increased to 3.74 bar^{-1} after 45 min thus showing an increase of quenching. After 90 min, there is no more change since the quenching process is already equili-

Table 3. Fit data of Stern-Volmer plots calculated for MOF-76(Eu) activated at temperatures T_{act} of 50 °C, 100 °C, 150 °C and 250 °C as well as methanol-exchanged MOF-76(Eu) at 250 °C.

T_{act}/°C	t/min	K_{SV}/bar^{-1}	R^2
50	3	3.47	0.9986
	45	3.74	0.9998
	90	3.74	0.9996
100	3	3.38	0.9995
	45	3.61	0.9998
	90	3.57	0.9998
150	3	23.6	0.9995
	45	23.7	0.9996
	90	23.3	0.9983
250	3	24.7	0.9963
	45	25.1	0.9972
	90	25.0	0.9975
250 (MeOH exchanged)	3	28.0	0.9987
	45	28.3	0.9990
	90	28.1	0.9987

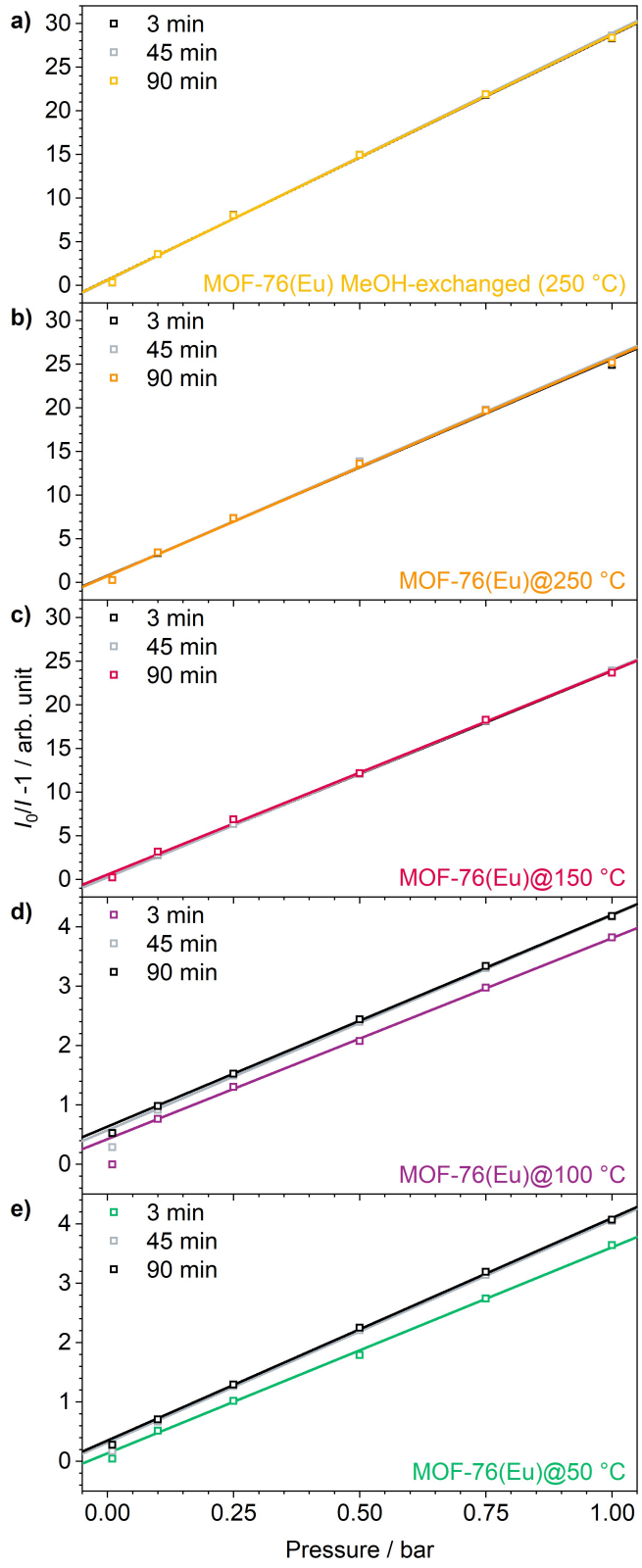

Figure 8. Comparison of time and activation condition dependent Stern-Volmer kinetics after dosing of oxygen for MOF-76(Eu) activated at 50 °C and 100 °C as well as 150 °C, 250 °C and methanol-exchanged at 250 °C. For MOF-76(Eu) activated at 50 °C and 100 °C, data recorded at 0.01 bar was not considered, because no equilibrium was reached at this oxygen pressure.

brated and therefore does not show significant changes to K_{SV}. Hence, the impact of activation also shows in the determination of K_{SV}, as the slow diffusion through the pores of MOF-76(Eu) insufficiently activated at 50 °C or 100 °C results in a slow quenching process. In comparison, MOF-76(Eu) activated at 150 °C (Figure 8a–c) and above, show a significantly increased K_{SV}, as result of the stronger quenching, e.g. 23.6 bar^{-1} after 3 min for MOF-76(Eu) activated at 150 °C. Furthermore, K_{SV} does not show a significant change over time, since the quenching process is finished within less than a second. K_{SV} is rather fluctuating around a certain value in this case which is already settled at the beginning of the measurement due to the fast diffusion of oxygen.

Reusability is another important property of a sensor besides sensitivity and response time. Consequently, cycling measurements usually are carried out to demonstrate if the initial photoluminescence emission intensity can be restored after multiple cycles. In this case, they were carried out to observe the influence of activation on the long-term stability of MOF-76(Eu) as an oxygen sensor and to test, if higher quenching occurs due to further removal of solvent over time. The samples were cycled between vacuum and oxygen atmosphere. After reaching the desired pressure, the sample was kept at the set pressure for 150 s before applying the next step. The total duration of the investigations varies due to the different time it takes to reach the desired pressures. Results of the cycling measurements are depicted in Figure 9. MOF-76(Eu) activated at temperatures of 150 °C and above (including methanol-exchanged sample, Figure 9a–c) shows a fast response and no decrease of the initial intensity after ten cycles. In contrast, MOF-76(Eu) activated at 50 °C and 100 °C (Figure 9d–e) shows reduction to 53.7 % and 65.3 % of its initial photoluminescence emission intensity in the vacuum step of the tenth cycle. Since this could be caused in part by the relatively short step holding time of 150 s, which is shorter than the response time of the sensor, another measurement of MOF-76(Eu) activated at 100 °C with an oxygen exposure time of 80 min and a vacuum step time of 30 min was carried out (Figure 10). The emission quenching reaches an equilibrium in the oxygen steps of the cycling measurements, but during vacuum steps the intensity cannot be fully recovered. This indicates that the oxygen cannot be fully removed from the pores again and the solvent is trapping it inside the pores by slowing down diffusion. In the following oxygen addition step, the emission intensity is quenched a little bit stronger than in the step before, as it was also observed in the ten-cycle measurement. Thus, a longer exposure to oxygen leads to a slowly ongoing diffusion of more oxygen into the pores. This also explains that the intensity in the second vacuum step is not fully recovered.

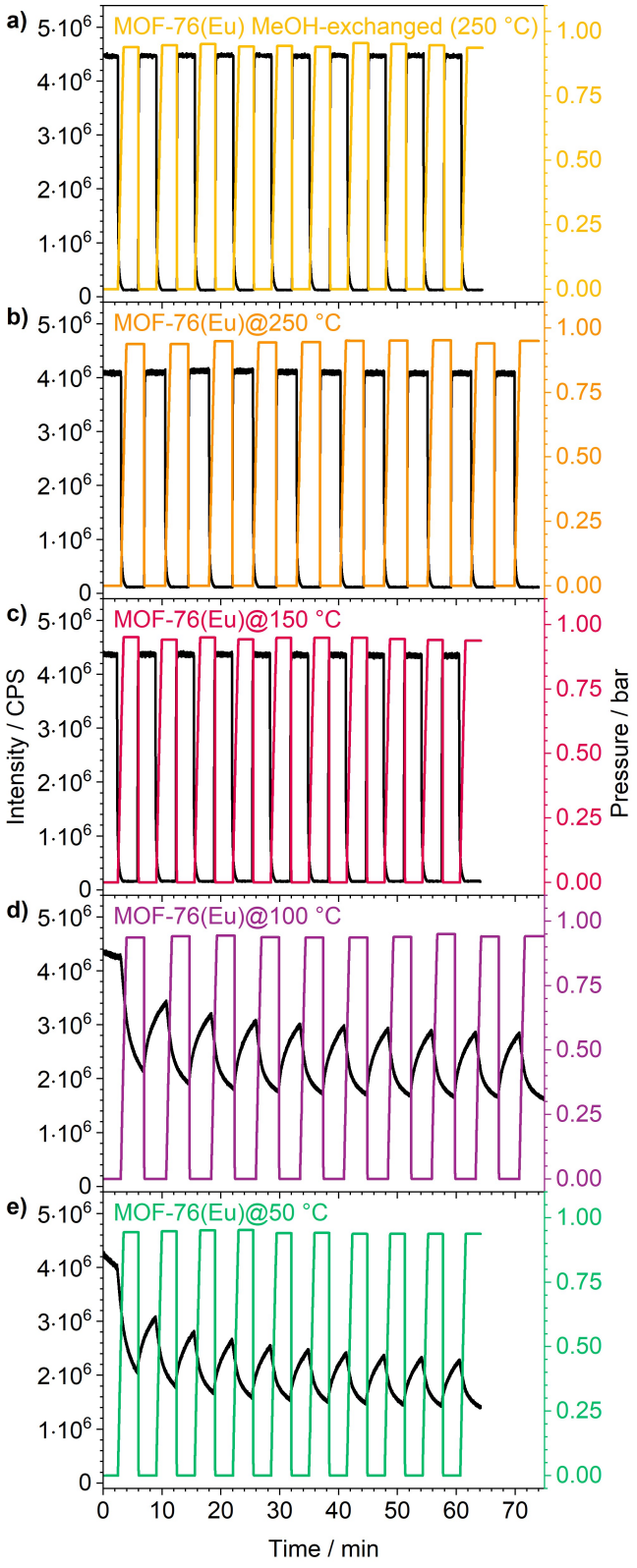

Figure 9. Cycling measurements of MOF-76(Eu) activated at different conditions. The length of the cycles varies due to different times required to reach the desired pressure.

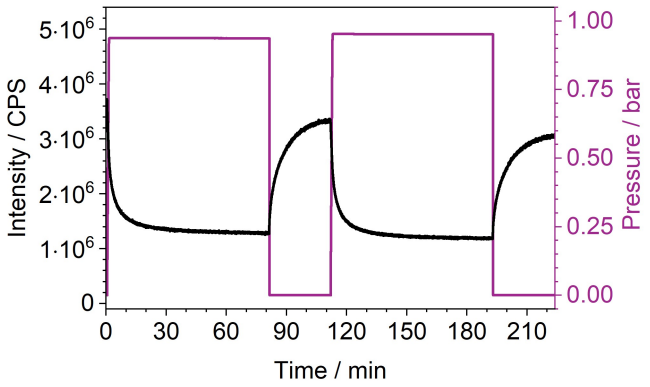

Figure 10. Oxygen cycling investigation of MOF-76(Eu)@100 °C with an oxygen exposure time of 80 min and a vacuum step length of 30 min.

Experimental

Synthetic Procedures

Synthesis of MOF-76(Eu): A procedure according to Rosi *et al.* was used and modified.[48] In a mixture of DMF and demineralized water (3 : 1, 60 mL), $Eu(NO_3)_3 \cdot 6H_2O$ (638 mg, 1.43 mmol; *abcr*, 99.9 %) and 1,3,5-benzenetricarboxylic acid (300 mg, 1.43 mmol; *abcr*, 98 %) were dissolved. Hydrochloric acid (0.5 mL, conc.) was added and the solution transferred to a pressure tube (*Ace Glass 8648-27, 120 mL, Front Seal Plug*). With a heating jacket (*Horst MA03078* with *HT MC11* controller) this solution was heated to 80 °C (heating/cooling ramp: 2 h/4 h) for 12 h. The product was obtained as colorless needles and vacuum-filtrated over a fritted glass crucible (Por. 4) and washed three times with DMF.

Activation of MOF-76(Eu): The as-synthesized MOF (100 mg) was transferred to a glass tube with Young valve. The tube was evacuated (0.001 mbar) and the sample heated to the desired temperature using a heating jacket (*Horst MA03078 with HT MC11 controller*) for 15 h. After this procedure the powders were transferred to an argon glovebox.

Analytical Investigations

X-ray powder diffraction: Structure of the synthesized MOF was characterized using a *PANalytical X'Pert Pro* diffractometer equipped with a *X'Celerator* detector. Measurements were carried out with angle ranges of 2θ from 5° to 60°, a step width of 0.033° and an exposure time of 150 s. Copper K_α radiation was used. Activated MOF-76(Eu) was prepared in an Ar glovebox using an inert sample holder that was sealed with *Kapton* foil. *Bruker DIFFRAC.EVA Version 5.2.0.5.* was used to perform a background correction on the measured powder diffractograms. Simulations of diffractograms were created with *CCDC Mercury 2021.3.0* from 5° to 60° with a step size of 0.02° and FWHM (full width at half maximum) of 0.1.

Photoluminescence spectroscopy: A *Horiba Jobin Yvon Fluorolog 3* equipped with a 450 W short-arc lamp (*USHIO*), a UV xenon flashlamp (*Excelitas FX-1102*), double-grated excitation and emission monochromators, a photomultiplier tube (*R928P*) and a TCSPC (time-correlated single-photon counting) upgrade was used to record photoluminescence excitation and emission spectra. The spectra were corrected for spectral response of monochromators and detectors with spectral corrections provided by the manufacturer. In addition, a correction for the spectral response of the lamp was performed for the excitation spectra with a photodiode

reference detector. An edge filter (*Newport*, cutoff wavelength: 495 nm) was used to cover the full spectral range. Emission intensity decays were measured using the *DataStation* software and fitted monoexponentially with *Decay Analysis Software 6*. The samples were prepared in air and filled into round quartz glass cuvettes.

Photoluminescence quantum yield was determined using another *Horiba Jobin Yvon Fluorolog 3* equipped with a 450 W short-arc lamp (*USHIO*), double-grated excitation and emission monochromators and a photomultiplier tube (*R928P*) combined with a *HORIBA Quanta-φ* integrating sphere (*F-3029*). The sample was prepared in ambient atmosphere and filled into a micro cell cuvette (*Starna 18-F/ST/C/Q/10*). Reference material (magnesium oxide) and sample were measured several times and the quantum yield with standard deviation calculated subsequently. Calibration of Integrating Sphere was checked by additional standards (sodium salicylate powder, $\lambda_{ex} = 340$ nm, $\lambda_{em} = 365$–600 nm; measured QY = 55.7(4)%, literature value: 53 %;[59] $[Eu_4(OAc)_{12}(phenylterpyridine)_2]$, $\lambda_{ex} = 310$ nm, $\lambda_{em} = 575$–720 nm; measured QY = 64.5(2.8) %, literature value: 57.9(3.9) %[60]).

Physisorption: A *Quantachrome Autosorb AS-1MP* was used to perform physisorption measurements using *AS1win* software. The activated MOFs were measured without further outgassing. N_2 (*Nippon gases*, 5.0) was used as adsorbate at 77 K. Surface areas were determined with the 5-point BET method using *ASiQwin version 5.2*. The linear section of the BET plot was determined via single-point BET method. The point showing the highest single-point BET surface area and the four preceding points were chosen for the 5-point BET method. Multi-point BET plots and related information can be found in the supporting information.

Elemental analysis: To determine the elemental composition of activated MOF-76(Eu), the powders were placed on a tin foil and pressed to a pellet. Measurements were carried out on an *Elementar Unicube*.

Thermal analysis: Differential thermal analysis and thermogravimetry were simultaneously measured using a NETZSCH STA-409-PC coupled with a QMS 403 Aëolos Quadro. Argon was used as protective gas with a flow rate of 20 $mL \cdot min^{-1}$ and as working gas with a flow rate of 30 $mL \cdot min^{-1}$. The samples (10–20 mg) were heated up to 1000 °C (ramp: 5 $°C \cdot min^{-1}$).

Oxygen sensing: The above-mentioned *Horiba Jobin Yvon Fluorolog 3* spectrometer used for quantum yield determinations was also used for the oxygen gas sensing measurements. The spectrometer was coupled to a physisorption device (*Quantachrome Autosorb AS-1MP*). Powders were placed in an L-shaped sample cell with a window made of *Suprasil* to prevent excitation or emission radiation from being absorbed by the glass. A glass fiber was attached to this window, allowing measurements to be made outside the spectrometer. O_2 and He were purchased from *Nippon Gases* and had a purity of 5.0.

First, the sample cell was flushed three times with He and evacuated to 10^{-7} bar to measure a reference emission spectrum. Then a physisorption analysis was started with p/p_0 points from 0.01 to 0.99. This measurement was performed at room temperature and p_0 was set to 760 mmHg to ensure that the points were collected at the desired absolute pressures. The two measurement PCs were connected in a local network and the program *AutoHotkey* was used to read the *Autosorb* log file from the *Fluorolog* PC and automatically start the collection of emission spectra when oxygen was dosed into the sample cell. Measurement of emission spectra was started with a time interval of 3 min. For samples showing a faster response towards oxygen the measurement was started before dosing of oxygen into the sample cell and the emission maximum of Eu^{3+} was measured every 0.1 s (corresponding to integration time). An edge filter (*Newport*, cutoff wavelength: 400 nm) was used.

Conclusions

In this work, an investigation on the influence of activation on luminescent oxygen sensing in MOF-76(Eu) was conducted that shows a strong impact of activation parameters on the overall performance of the sensor regarding sensitivity through quenching efficiency and response time. The archetype metal–organic framework MOF-76(Eu) is a potential optical oxygen sensor, whether activated or not, but activation is vital to reach the full potential of the sensor. To show this, MOF-76(Eu) was activated at different temperatures of 50 °C, 100 °C, 150 °C and 250 °C, and was additionally DMF/methanol-exchanged before activation at 250 °C. The different temperatures result in a different degree of solvent removal/residues from the synthesis in the MOF pores. Physisorption analysis confirmed this exhibiting no porosity for N_2 adsorption and low surface area for MOF-76(Eu) activated up to 100 °C. In contrast, activation at 150 °C and above showed accessible microporosity and much higher surface areas up to 768 $m^2 g^{-1}$ for methanol-exchanged MOF-76(Eu). These observations correlate well with the oxygen sensing results in term of quenching rate and response time. Due to the low accessibility of the pores, an activation at 50 °C or 100 °C leads to a medium quenching rate of about 80 % within 30 min. Residual solvent in the pores slows the diffusion of oxygen through the occupied pores down. Activating MOF-76(Eu) at 150 °C and above leads to a significant change, with a maximum for the methanol-exchanged MOF-76(Eu) activated at 250 °C accompanied by the highest quenching rate of 98.6 %. As result of successful activation and removal of the solvent, the pores are more easily accessible leading to a very short response time of only 0.2 s. Activation thereby marks the difference between a sensor suitable for "on-the-fly" sensing by the eye due to the short response time. Moreover, the residual solvent influences Stern-Volmer kinetics and results in incorrect values for Stern-Vomer constants calculated from photoluminescence spectra collected before equilibration of the system. Since the Stern-Volmer constant is considered to quantify the strength of quenching, this underlines the importance of considering the activation as key parameter for oxygen gas sensing. Cycling measurements showed that sufficient activation is also important for the reusability of MOF-76(Eu) as oxygen sensor. MOF-76(Eu) activated at 150 °C and 250 °C (including methanol-exchange) showed reversibility of the initial intensity after ten cycles, whereas activation at temperatures below 150 °C is not suitable to recover the initial PL intensity in vacuum of the first cycle. Overall, the activation of a MOF is not only important for reaching high surface areas, in oxygen gas sensing it plays a key role for several highly relevant sensing parameters ranging from sensitivity

to response time and even cyclability/reusability. MOF activation thereby defines the performance of the sensor for this kind of optical sensing.

Supporting Information

The supporting information contains further information on the BET and photoluminescence data. The authors have cited additional references within the Supporting Information.[49,53,61–65]

Acknowledgements

The authors gratefully acknowledge the Deutsche Forschungsgemeinschaft for supporting this work within the priority program SPP1928 and the project MU-1562/13-1 "Optical Sensing and Energy Transfer in Luminescent and Conductive COORNET Mixed-Matrix Membranes". Open Access funding enabled and organized by Projekt DEAL.

Conflict of Interests

The authors declare no conflict of interest.

Data Availability Statement

The data that support the findings of this study are available in the supplementary material of this article.

Keywords: oxygen sensing · metal–organic frameworks · luminescence · optical sensing · activation

[1] H. Yuan, N. Li, W. Fan, H. Cai, D. Zhao, *Adv. Sci.* **2022**, *9*, 2104374.
[2] H. Nazemi, A. Joseph, J. Park, A. Emadi, *Sensors* **2019**, *19*, 1285.
[3] Y. Zhao, Y. Liu, B. Han, M. Wang, Q. Wang, Y. Zhang, *Coord. Chem. Rev.* **2023**, *493*, 215297.
[4] T. Kasper, M. Pavan, K. Müller-Buschbaum, *J. Mater. Chem. A* **2023**, DOI 10.1039/D3TA05209E.
[5] M. Eltermann, K. Utt, S. Lange, R. Jaaniso, *Opt. Mater.* **2016**, *51*, 24–30.
[6] X. Y. Dong, Y. Si, J. S. Yang, C. Zhang, Z. Han, P. Luo, Z. Y. Wang, S. Q. Zang, T. C. W. Mak, *Nat. Commun.* **2020**, *11*, 1–9.
[7] Y. Tang, J. Chen, H. Wu, J. Yu, J. Jia, W. Xu, Y. Fu, Q. He, H. Cao, J. Cheng, *Dyes Pigm.* **2020**, *172*, 107798.
[8] J. Sipior, S. Bambot, M. Romauld, G. M. Carter, J. R. Lakowicz, G. Rao, *Anal. Biochem.* **1995**, *227*, 309–318.
[9] R. Haldar, S. Bhattacharyya, T. K. Maji, *J. Chem. Sci.* **2020**, *132*, 99.
[10] S. K. Pandey, K.-H. Kim, K.-T. Tang, *TrAC Trends Anal. Chem.* **2012**, *32*, 87–99.
[11] F. I. M. Ali, F. Awwad, Y. E. Greish, S. T. Mahmoud, *IEEE Sens. J.* **2019**, *19*, 2394–2407.
[12] F. A. A. Nugroho, P. Bai, I. Darmadi, G. W. Castellanos, J. Fritzsche, C. Langhammer, J. Gómez Rivas, A. Baldi, *Nat. Commun.* **2022**, *13*, 5737.
[13] Q. Yao, G. Ren, K. Xu, L. Zhu, H. Khan, M. Mohiuddin, M. W. Khan, B. Y. Zhang, A. Jannat, F. Haque, S. Z. Reza, Y. Wang, X. Wen, A. Mitchell, J. Z. Ou, *Adv. Opt. Mater.* **2019**, *7*, 1901383.
[14] F. Schönfeld, L. V. Meyer, F. Mühlbach, S. H. Zottnick, K. Müller-Buschbaum, *J. Mater. Chem. C* **2018**, *6*, 2588–2595.
[15] X. Wang, K. Batra, G. Clavier, G. Maurin, B. Ding, A. Tissot, C. Serre, *Chem. Eur. J.* **2023**, *29*, e202203136.
[16] A. Ghosh, N. Sikdar, T. K. Maji, *J. Mater. Chem. C* **2022**, *10*, 7558–7566.
[17] I. Yoshiya, Y. Shimada, K. Tanaka, *Med. Biol. Eng. Comput.* **1980**, *18*, 27–32.
[18] S. Hanf, R. Keiner, D. Yan, J. Popp, T. Frosch, *Anal. Chem.* **2014**, *86*, 5278–5285.
[19] S. R. Morrison, *Sens. Actuators* **1987**, *12*, 425–440.
[20] H. Nakai, J. Seo, K. Kitagawa, T. Goto, T. Matsumoto, S. Ogo, *Dalton Trans.* **2016**, *45*, 9492–9496.
[21] R.-B. Lin, F. Li, S.-Y. Liu, X.-L. Qi, J.-P. Zhang, X.-M. Chen, *Angew. Chem. Int. Ed.* **2013**, *52*, 13429–13433.
[22] X. Wang, Y. Jiang, A. Tissot, C. Serre, *Coord. Chem. Rev.* **2023**, *497*, 215454.
[23] M. Bregnhøj, K. Strunge, R. J. Sørensen, M. Ströbele, T. Hummel, H.-J. Meyer, F. Jensen, P. R. Ogilby, *J. Phys. Chem. A* **2019**, *123*, 1730–1739.
[24] L. Riehl, A. Seyboldt, M. Ströbele, D. Enseling, T. Jüstel, M. Westberg, P. R. Ogilby, H.-J. Meyer, *Dalton Trans.* **2016**, *45*, 15500–15506.
[25] D. J. Osborn, G. L. Baker, R. N. Ghosh, *J. Sol-Gel Sci. Technol.* **2005**, *36*, 5–10.
[26] L. V. Meyer, F. Schönfeld, A. Zurawski, M. Mai, C. Feldmann, K. Müller-Buschbaum, *Dalton Trans.* **2015**, *44*, 4070–4079.
[27] X. Y. Xu, B. Yan, *J. Mater. Chem. C* **2016**, *4*, 8514–8521.
[28] J. W. Ye, J. M. Lin, Z. W. Mo, C. T. He, H. L. Zhou, J. P. Zhang, X. M. Chen, *Inorg. Chem.* **2017**, *56*, 4238–4243.
[29] C. Y. Zhu, Z. Wang, J. T. Mo, Y. N. Fan, M. Pan, *J. Mater. Chem. C* **2020**, *8*, 9916–9922.
[30] T. Xia, L. Jiang, J. Zhang, Y. Wan, Y. Yang, J. Gan, Y. Cui, Z. Yang, G. Qian, *Microporous Mesoporous Mater.* **2020**, *305*, 110396.
[31] T. Burger, C. Winkler, I. Dalfen, C. Slugovc, S. M. Borisov, *J. Mater. Chem. C* **2021**, *9*, 17099–17112.
[32] T. Burger, M. V. Hernández, C. Carbonell, J. Rattenberger, H. Wiltsche, P. Falcaro, C. Slugovc, S. M. Borisov, *ACS Appl. Nano Mater.* **2023**, *6*, 248–260.
[33] S.-Y. Liu, X.-L. Qi, R.-B. Lin, X.-N. Cheng, P.-Q. Liao, J.-P. Zhang, X.-M. Chen, *Adv. Funct. Mater.* **2014**, *24*, 5866–5872.
[34] Z. Dou, J. Yu, Y. Cui, Y. Yang, Z. Wang, D. Yang, G. Qian, *J. Am. Chem. Soc.* **2014**, *136*, 5527–5530.
[35] F. Y. Yi, D. Chen, M. K. Wu, L. Han, H. L. Jiang, *ChemPlusChem* **2016**, *81*, 675–690.
[36] S. N. Nangare, A. G. Patil, S. M. Chandankar, P. O. Patil, *J. Nanostructure Chem.* **2023**, *13*, 197–242.
[37] X. L. Qi, S. Y. Liu, R. B. Lin, P. Q. Liao, J. W. Ye, Z. Lai, Y. Guan, X. N. Cheng, J. P. Zhang, X. M. Chen, *Chem. Commun.* **2013**, *49*, 6864–6866.
[38] S. M. Barrett, C. Wang, W. Lin, *J. Mater. Chem.* **2012**, *22*, 10329–10334.
[39] Y.-T. Chen, C.-Y. Lin, G.-H. Lee, M.-L. Ho, *CrystEngComm* **2015**, *17*, 2129–2140.
[40] M. L. Ho, Y. A. Chen, T. C. Chen, P. J. Chang, Y. P. Yu, K. Y. Cheng, C. H. Shih, G. H. Lee, H. S. Sheu, *Dalton Trans.* **2012**, *41*, 2592–2600.
[41] Z. Xie, L. Ma, K. E. DeKrafft, A. Jin, W. Lin, *J. Am. Chem. Soc.* **2010**, *132*, 922–923.
[42] T. O. Knedel, S. Buss, I. Maisuls, C. G. Daniliuc, C. Schlüsener, P. Brandt, O. Weingart, A. Vollrath, C. Janiak, C. A. Strassert, *Inorg. Chem.* **2020**, *59*, 7252–7264.
[43] X. Qiao, Z. Ma, L. Si, W. Ding, G. Xu, *Sens. Actuators B* **2019**, *299*, 126978.
[44] J. An, C. M. Shade, D. A. Chengelis-Czegan, S. Petoud, N. L. Rosi, *J. Am. Chem. Soc.* **2011**, *133*, 1220–1223.
[45] H. Weng, X. Y. Xu, B. Yan, *J. Colloid Interface Sci.* **2017**, *502*, 8–15.
[46] F. Gao, F. Luo, X. Chen, W. Yao, J. Yin, Z. Yao, L. Wang, *Microchim. Acta* **2009**, *166*, 163–167.
[47] D.-K. Nguyen, J.-H. Lee, T. L.-H. Doan, T.-B. Nguyen, S. Park, S. S. Kim, B. T. Phan, *Appl. Surf. Sci.* **2020**, *523*, 146487.
[48] N. L. Rosi, J. Kim, M. Eddaoudi, B. Chen, M. O'Keeffe, O. M. Yaghi, *J. Am. Chem. Soc.* **2005**, *127*, 1504–1518.
[49] J. Yang, Q. Yue, G.-D. Li, J.-J. Cao, G.-H. Li, J.-S. Chen, *Inorg. Chem.* **2006**, *45*, 2857–2865.
[50] J. Hafizovic, M. Bjørgen, U. Olsbye, P. D. C. Dietzel, S. Bordiga, C. Prestipino, C. Lamberti, K. P. Lillerud, *J. Am. Chem. Soc.* **2007**, *129*, 3612–3620.
[51] C. Serre, C. Mellot-Draznieks, S. Surblé, N. Audebrand, Y. Filinchuk, G. Férey, *Science* **2007**, *315*, 1828–1831.
[52] T. Stumpf, M. Bolte, *Acta Crystallogr. Sect. E* **2001**, *57*, i10–i11.
[53] D. J. Duchamp, R. E. Marsh, *Acta Crystallogr. Sect. B* **1969**, *25*, 5–19.
[54] T.-W. Duan, B. Yan, *J. Mater. Chem. C* **2014**, *2*, 5098–5104.

[55] X. Yang, X. Lin, Y. Zhao, Y. S. Zhao, D. Yan, *Angew. Chem.* **2017**, *129*, 7961–7965.
[56] A. Garg, M. Almáši, R. Saini, D. R. Paul, A. Sharma, A. Jain, I. P. Jain, *Environ. Sci. Pollut. Res. Int.* **2022**, DOI 10.1007/s11356-022-21290-y.
[57] T. Kiyonaga, M. Higuchi, T. Kajiwara, Y. Takashima, J. Duan, K. Nagashima, S. Kitagawa, *Chem. Commun.* **2015**, *51*, 2728–2730.
[58] O. Stern, M. Volmer, *Phys. Z.* **1919**, *20*, 183–188.
[59] M. S. Wrighton, D. S. Ginley, D. L. Morse, *J. Phys. Chem.* **1974**, *78*, 2229–2233.
[60] A. E. Sedykh, M. Becker, M. T. Seuffert, D. Heuler, M. Maxeiner, D. G. Kurth, C. E. Housecroft, E. C. Constable, K. Müller-Buschbaum, *ChemPhotoChem* **2023**, *7*, e202200244.
[61] S. Øien, D. Wragg, H. Reinsch, S. Svelle, S. Bordiga, C. Lamberti, K. P. Lillerud, *Cryst. Growth Des.* **2014**, *14*, 5370–5372.
[62] C. Volkringer, M. Meddouri, T. Loiseau, N. Guillou, J. Marrot, G. Férey, M. Haouas, F. Taulelle, N. Audebrand, M. Latroche, *Inorg. Chem.* **2008**, *47*, 11892–11901.
[63] G. Férey, C. Serre, C. Mellot-Draznieks, F. Millange, S. Surblé, J. Dutour, I. Margiolaki, *Angew. Chem. Int. Ed.* **2004**, *43*, 6296–6301.
[64] I. Senkovska, F. Hoffmann, M. Fröba, J. Getzschmann, W. Böhlmann, S. Kaskel, *Microporous Mesoporous Mater.* **2009**, *122*, 93–98.
[65] R. Borjas Nevarez, S. M. Balasekaran, E. Kim, P. Weck, F. Poineau, *Acta Crystallogr. Sect. C* **2018**, *74*, 307–311.

Manuscript received: December 12, 2023
Revised manuscript received: March 9, 2024
Accepted manuscript online: March 20, 2024
Version of record online: May 26, 2024